



# Organization scale of photospheric magnetic imbalance in coronal holes

Matteo Cantoresi<sup>1,2</sup> · Francesco Berrilli<sup>1</sup> · Fabio Lepreti<sup>3</sup>

Received: 3 July 2023 / Accepted: 19 July 2023 / Published online: 13 September 2023  
© The Author(s) 2023

## Abstract

To investigate the statistical properties of the photospheric magnetic fields underlying coronal holes (CHs) and “normal” coronal regions a classical technique, the signed measure, is used. This technique allows to characterize the scaling behavior and the topology of sign-oscillating magnetic structures in selected regions of line of sight (LoS) magnetograms recorded by the Heliosismic Magnetic Imager on board of the Solar Dynamic Observatory (SDO/HMI). To this end we have compared the properties of the photospheric magnetic field underlying 60 CHs and 60 non-coronal holes (NCHs). In particular, in addition to having studied distributions and momenta of photospheric magnetic fields associated to the selected regions, we have performed the sign singularity analysis computing the cancellation functions of the highly fluctuating photospheric magnetic fields. We have found that photospheric magnetic fields associated to CHs are imbalanced in the sign and that this imbalance emerges mainly at the supergranular scales.

**Keywords** Sun: photosphere · Sun: magnetic fields · Sun: coronal holes (CHs) · Techniques: image processing

## 1 Introduction

The photospheric magnetic fields govern the magnetic dynamic of the entire solar atmosphere and therefore of the corona (Wiegelmann et al. 2014). Indeed, the coronal magnetic field evolves mainly in response to the emergence and evolution of the field on the solar surface. This field,

controlled by large-scale advection flows, differential rotation and meridional circulation (Mackay and Yeates 2012), and multiscale plasma flows associated with turbulent convection (Berrilli et al. 2013, 2014; Scardigli et al. 2021), continuously reconfigures the topology of the coronal magnetic arches possibly producing processes of instability and magnetic reconnection leading to explosive events such as flare and coronal mass ejections (CMEs). Solar flares and CMEs are events that can be related to extreme space weather phenomena (Cicogna et al. 2021; Napoletano et al. 2022; Plutino et al. 2023). For this reason they are of fundamental interest both for research in space physics and for services that have to mitigate extreme space events (Plainaki et al. 2020).

In the context of space weather, an equally important component is the high-speed solar wind. Solar wind of different speeds and densities is produced by different solar structures and regions. The high-speed component of the solar wind, ranging from 500 to 800 kms per second, is produced by CHs which appear as dark or poorly active solar regions when observed in extreme ultraviolet (EUV) or soft X-ray (SXR) on the solar disk or above the solar limb (Cranmer 2009).

A relevant feature of the CHs is that the cospatial photospheric magnetograms typically show a dominant magnetic

---

This paper belongs to the Topical collection “Frontiers in Italian studies on Space Weather and Space Climate”, that includes papers written on the occasion of the Second National Congress of SWiCo, “Space Weather Italian Community”, held on February 9–11 2022 in Rome’ at ASI, “Agenzia Spaziale Italiana”.

---

✉ Francesco Berrilli  
francesco.berrilli@roma2.infn.it

Matteo Cantoresi  
cantoresi.1668918@studenti.uniroma1.it

Fabio Lepreti  
fabio.lepreti@unicat.it

<sup>1</sup> Dipartimento di Fisica, Università di Roma Tor Vergata, Viale Ricerca Scientifica, 1, 00133 Rome, Italy

<sup>2</sup> Dipartimento di Fisica, Università di Roma La Sapienza, Piazzale Aldo Moro, 2, 00185 Rome, Italy

<sup>3</sup> Dipartimento di Fisica, Università della Calabria, Ponte Pietro Bucci, 31c, 87036 Arcavacata di Rende, CS, Italy

polarity, i.e. an imbalance in the magnetic flux distribution (Cranmer 2009; Wang 2009). The dominant magnetic polarity results in magnetic field lines that do not close in the proximity of the Sun, but reach far into interplanetary space. Thus, they are often referred to as “open magnetic field lines”. High-speed solar wind streams are formed by plasma which, due to the open magnetic field topology originating from photospheric magnetic flux imbalance, is not confined into the lower atmospheric regions and flows freely in interplanetary space.

Assuming conservation of open flux, Fisk (2005) presented a theoretical model in which regions with a reduced flux emergence rate of bipoles exist as compared to usual Quiet Sun (QS) regions. Open magnetic flux, due to interchange reconnection, accumulate in these areas, forming CHs. Abramenko et al. (2006) have compared the flux emergence rate in QSs with CHs, and found a lower emergence rate in the latter. However, such differences can be caused by other factors such as field imbalance (Hagenaar et al. 2006) or instrumental effects (Wang 2020). About the origin of the CHs, Karachik et al. (2010) have suggested, studying 4 CHs, that they originate from magnetic fields associated with active decaying regions. Whereas, Hofmeister et al. (2017) reported that the magnetic field in the coronal holes is clustered in small localized regions, mostly located in the supergranular network.

The long term evolution of a CH has been investigated by Heinemann et al. (2018b). The authors observed over 360° by observations from the Sun-Earth line as well as STEREO-A and STEREO-B satellites. During the CH area evolution, three phases are identified: a growing, a maximum and a decaying phase. The area evolution is found to be well correlated with variations of the distribution of the magnetic fields inside the CH and the flux tubes (FTs) number, in particular for what regards the strongest. Thus changes in the magnetic field are linked to CH area variations. Furthermore, Heinemann et al. (2018a) have studied the same CH and have found that solar wind peak velocity is linked to CH area variations and (thus) magnetic fields distribution. Consequently the evolution of this CH is driven mainly by FTs, in particular the strongest. These FTs could be the footpoints of the coronal funnels where the fast solar wind is generated. These seem rooted in the supergranular network. In this specific case of study a correlation has been found between CH area and CH magnetic flux density, while in Heinemann et al. (2020), studying a larger statistics of CHs, authors find that these two quantities are independent. More recently, Hofmeister et al. (2019) studied the lifetimes of magnetic elements in 98 CHs. They have found four classes, based on their average lifetime: related to the granulation, mesogranulation, supergranulation and long lived magnetic field elements (which live more than 40 h). It is shown that almost all the imbalance of the magnetic flux of CHs (68%)

arises from the long lived magnetic elements not associated to any convective (temporal) scale. They also found a slight imbalance in the magnetic fields not comprehended in the magnetic elements. Thus it is hypothesized that some mechanism relates long lived elements and this slightly imbalanced background. Also here it seems reasonable to think that these long lived magnetic elements are the footpoints of the funnels.

One of the goals of this work is to systematically examine how the cancellation exponents differ in photospheric magnetograms associated with CH and QS regions. This technique will allow us to measure the scales at which this imbalance emerges, providing information about the organization scale of the footpoints of coronal funnels in CHs. Furthermore, the analysis of the moments in the distributions associated to the different regions will allow to study the imbalance of the magnetic flux.

## 2 Method

### 2.1 The sign-singular measure

The photospheric magnetograms obtained along the line-of-sight (LoS) show outward and inward fluctuations of flux orientation that can be assimilated to positive and negative sign fluctuations, both in space and in time. Limiting in our case the analysis to spatial positive (outward) and negative (inward) flux fluctuations, which occur at different spatial scales, we can say that a form of singularity exists in photospheric magnetograms. This behavior is known as sign singularity and is the basis of the theory of sign-singular measure (Zhai et al. 2019). This technique was introduced by Ott et al. (1992) and applied for the first time to the multiscale measurement of the solar magnetic field by Ruzmaikin et al. (1993). Subsequently, the technique was used to characterize the multiscale and complexity properties of solar and heliophysical magnetism (e.g., Cadavid et al. 1994; Carbone and Bruno 1997; Consolini and Lui 1999; Sorriso-Valvo et al. 2003, 2015; Consolini et al. 2021).

The signed measure (e.g. Ott et al. 1992; Sorriso-Valvo et al. 2015) of a field  $f(r)$  can be defined on a  $d$ -dimensional domain  $Q(L)$  of size  $L$ . Let  $Q_i(l) \subset Q(L)$  be a partition of  $Q(L)$  in disjoint subsets of size  $l$ . Then, for each scale  $l$  and for each disjoint set of boxes  $Q_i(l)$ , the signed measure is:

$$\mu_i(l) = \frac{\int_{Q_i(l)} dr f(r)}{\int_{Q(L)} dr |f(r)|}. \quad (1)$$

Typically, when the size of the subset  $Q_i(l)$  is large, cancellations between small structures of opposite sign occur within each box, resulting in small contribution to the signed measure.

It is important to note that in our case study, this behaviour is expected in quiet or ephemeral solar regions, while it should not occur in coronal holes where we expect an imbalance in the magnetic field distribution. As the boxes become smaller and reach the typical size of the structures, each one is more likely to contain one single, sign-defined structure, reducing the level of cancellations. The way this happens can be statistically characterized through the cancellation function

$$\chi(l) = \sum_{Q_i(l)} |\mu_i(l)|. \quad (2)$$

It holds information on the sign of the field fluctuations. The measure is called sign singular if it changes sign on arbitrarily fine scales. For fields which satisfy the property of self similarity, Eq. 2 follows a power law (Lawrence et al. 1993):

$$\chi(l) \propto l^{-k}. \quad (3)$$

The power law index  $k$  is called cancellation index. It is possible to calculate the cancellation function from data and obtain the cancellation exponent with a linear fitting procedure in log–log scale. The cancellation exponent  $k$  represents an effective measure of the efficiency of the field cancellations.

In particular for a smooth field<sup>1</sup>  $k = 0$  while for a Brownian noise  $k = d/2$ , where  $d$  is the typical dimension of the problem considered. Cancellation exponents between those two limiting values indicate the presence of smooth structures embedded in random fluctuations.

These structures could be associated to scale dependent signed fluctuations of the fields.  $k > d/2$  would indicate a strong cancellation associated to opposite fields (in the case of the photospheric magnetic fields a bipole).

## 2.2 Analysis

The aim of our analysis is to study the properties of the photospheric magnetic fields associated to different regions of interest (RoIs) of the solar atmosphere, i.e. coronal holes and regions outside of coronal holes and active regions (we call them 'Non CHs' or NCHs).

To define the regions of interest (CHs and NCHs) on which to perform the analysis, we used SDO/AIA and SDO/HMI data (Pesnell et al. 2012). The HMI instrument, from polarization measurements, derives full disk maps, including magnetic LoS maps used in this paper. While, the AIA instrument observes at 10 wavelengths showing the Sun, from the photosphere to the corona, at various temperatures of its atmosphere (from about 5000 K to about 2.5 MK).

SDO/AIA images are used to identify coronal holes and quiet solar regions. More in detail, the datasets used in this work are SDO/HMI LoS and low cadence (720 s) magnetograms, both for CHs and NCHs, and SDO/AIA at 1930 nm filtergrams.

We have extracted CHs boundaries from AIA images using the SpoCA routine (Verbeeck et al. 2014) and projected them to the HMI field of view.

For our analysis we have used 60 different magnetograms associated to equatorial CHs close to the central meridian, in order to reduce geometrical effects, and 60 magnetograms associated to NCH regions. Magnetograms have been resized with respect to the size of the Sun at the aphe- lium; LoS magnetic fields have been re-projected. The chosen HMI sub-regions in which the analysis is made are the largest squares inscribable inside the selected CHs. NCHs have been extracted from HMI LoS magnetograms considering squared regions where neither CHs nor ARs are present (Fig. 1). The sub-regions selected have the same dimensions of the sub-regions selected for the CH analysis.

The sub-regions considered have sides of dimensions which range from 180 to 540 pixels, corresponding to about 70–200 Mm, respectively.

We studied the cancellation function (Eq. 2) for all sub-regions belonging to the 60 different magnetograms associated to equatorial CHs and to the 60 magnetograms associated to NCH regions. The calculation of the cancellation exponent was performed on all the sub-regions through a linear fit, in a suitable interval, of the cancellation function plotted in a log–log scale. The fit is performed considering the 7 point interval of the cancellation function which maximizes the Pearson linearity coefficient, excluding the first two scales (1 and 2 pixels) for the Nyquist frequency limit. In Fig. 2 we report (in a log–log scale) the cancellation functions estimated for two specific RoIs belonging to a CH (upper panel) and a NCH (bottom panel). It is also reported (in red) the linear fit to estimate the cancellation exponent ( $k$ ).

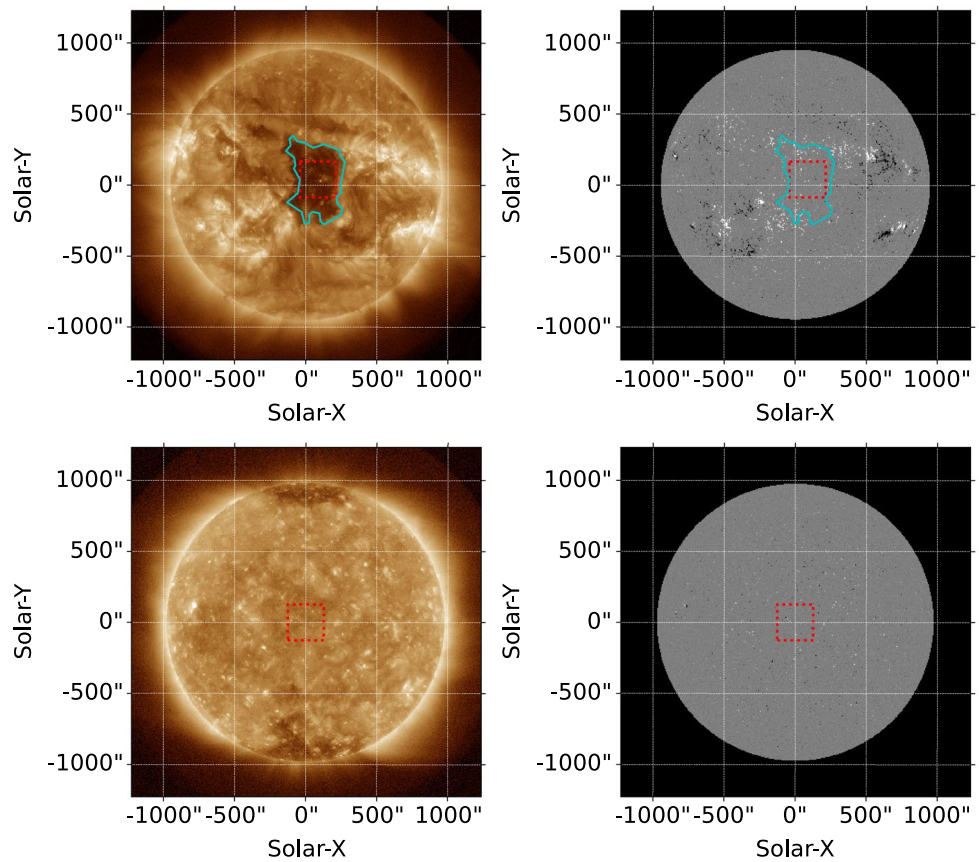
In Fig. 3 we report the distributions of the  $k$  calculated for magnetic fields of RoIs belonging to CH and NCH (upper and bottom panels, respectively), reported respectively in Tables 1 and 2.

We have reported, in the previous sections, that the photospheric magnetograms associated with CHs present an imbalance of the magnetic field sign, i.e. they show a dominant (outward or inward, it doesn't matter) magnetic field sign. In order to study the distributions associated with the selected RoIs (i.e., CHs and NCHs) we decided to use the moments of the distributions.

We have analysed the distributions of magnetic fields associated to CHs and NCHs estimating the mean, the first moment (M1), and the skewness, the third moment (M3),

<sup>1</sup> In a completely smooth field there is not sign singularity.

**Fig. 1** Selected RoIs on AIA (left column) and HMI (right column) magnetograms, both from the CH (upper row) and the NCH (bottom row) regions, for two specific events (CH nr.2 and NCH nr.59 in Tables 1 and 2, respectively). The boundaries of the CH is indicated in blue; the selected RoI in dotted red. HMI magnetograms have been reprojected to AIA filtegrams for comparison



which gives us information about the lack of symmetry (balance) of the distribution.

The noise level (at central disk) of the HMI LoS 720 s data product series is around 5 Gauss (Couvidat et al. 2016; Hofmeister et al. 2017); consequently the magnetogram pixels with magnetic flux density below 15 Gauss (3 times the noise level) have been removed.

The results of the analysis of the momenta (M1 and M3) of the distribution of magnetic fields associated to CHs and NCHs are reported in Figs. 4 and 5 (see Tables 1 and 2, respectively). Since we have said that the dominant sign of the magnetic field value is not relevant, for simplicity we have reported in the figures the absolute values of M1 and M3 for the regions analyzed.

### 3 Discussion

As we have said the signed measure is a technique which provides us with information about the scaling behaviour of the oscillations of the photospheric magnetic fields. This is particularly evident in Fig. 2 where we report the cancellation functions estimated for two specific regions (with the same dimension) associated to a CH and to a NCH RoI. For these two specific cases we obtain that  $k_{\text{CH}} = 0.39 \pm 0.05$

and  $k_{\text{NCH}} = 0.51 \pm 0.11$ , thus the field of the CH oscillates less with respect to the NCH case, as expected. We can also observe that in the case of CHs, as for the CH nr.19 shown in the upper panel of Fig. 2, the cancellation function assumes a constant value from around 30 Mm (the supergranular scale of the Sun) indicating that from this specific scale the sign of the magnetic signal does not oscillate any more (i.e. the field becomes smooth).

We report in Fig. 3 the distribution of the cancellation exponents calculated for both the CHs (upper panel) and the NCHs (bottom panel). From the comparison of the two distributions we conclude that in the case of the NCH higher values of  $k$  are more probable with respect to the CH case. As we have discussed, this implies that photospheric magnetic fields associated to NCH are more singular in the sign with respect to CH photospheric magnetic fields.

What we observe therefore, as it is possible to see in the example reported in Fig. 2 where at the largest spatial scales the CH cancellation function shows a plateau, i.e., it assumes a constant value, is that on these scales there is no more magnetic field cancellation and consequently the field orientation remains fixed, its sign remains constant and is no longer singular.

In order to estimate the typical scale at which the plateau begins we have decided to use the numerical derivative

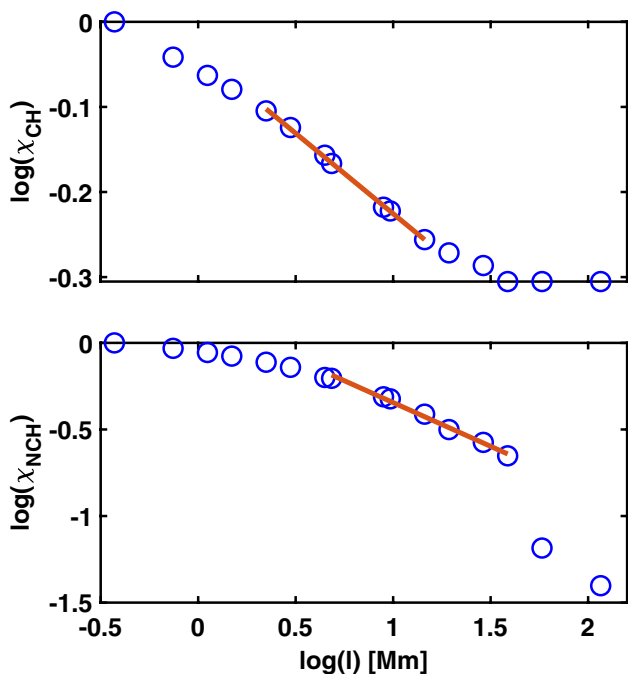


**Fig. 2** We show in this figure two cancellation functions calculated for a typical CH ( $\chi_{CH}(l)$ , CH nr.19), upper panel, and a typical NCH ( $\chi_{NCH}(l)$ , NCH nr.45), lower panel, in function of the scale  $l$ . Functions are shown in log-log scale. The reader must pay attention to the different ranges of the ordinate axis. In red it is indicated the linear fit to estimate the cancellation exponent ( $k$ )

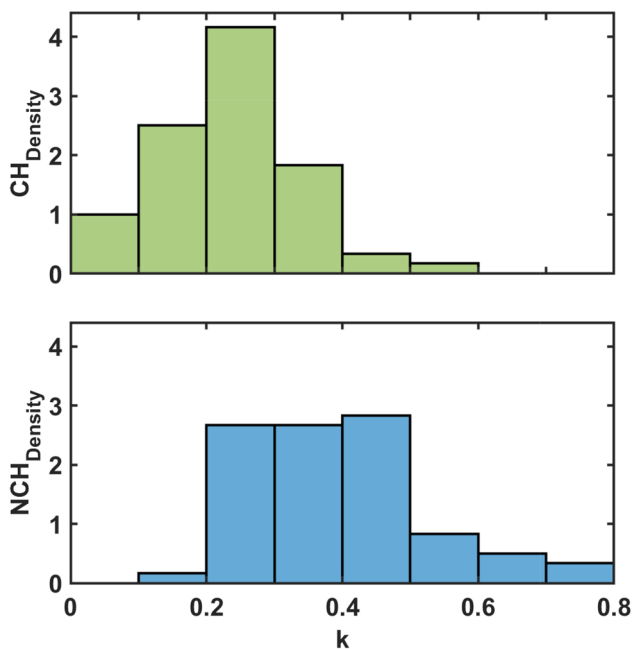


**Fig. 3** PDF of the cancellation exponents estimated for CHs (upper panel) and NCHs (bottom panel)

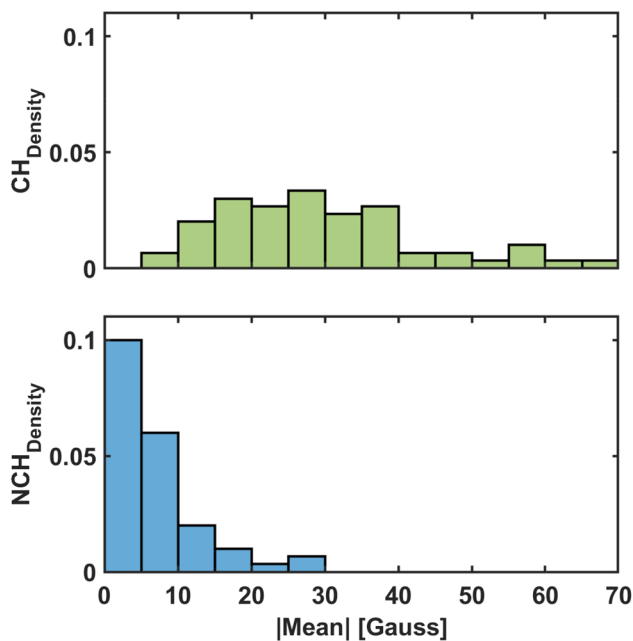


**Fig. 4** PDF of the means of photospheric magnetic fields associated to CHs (upper panel) and NCHs (bottom panel)

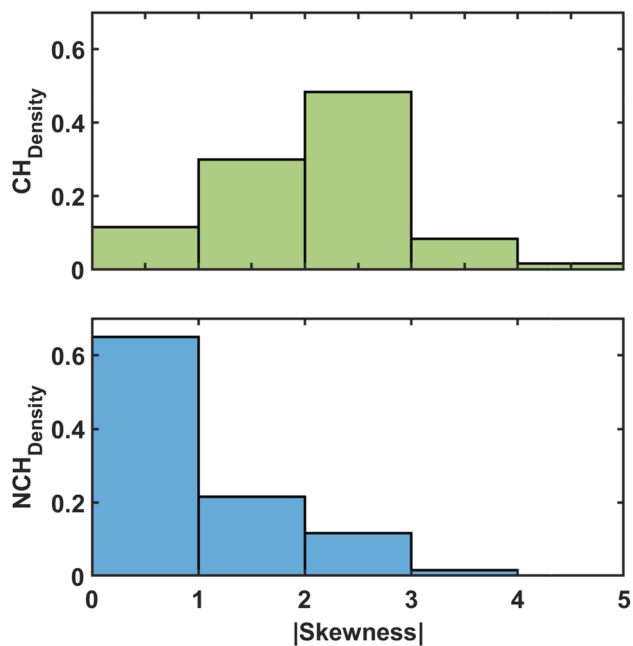


**Fig. 5** PDF of the skewness of photospheric magnetic fields associated to CHs (upper panel) and NCHs (bottom panel)

of the cancellation function. We define plateau all points (scales) that have a numerical derivative less than a fixed threshold. From the analysis carried out on the various cancellation functions we have estimated that an effective value of the threshold is equal to  $10^{-4}$ . Considering smaller values

**Table 1** Analyzed coronal holes

CH nr	Date (yyyy. mm.dd)	Cancellation expo- nent $k$	$\Delta$	Mean (G)	Skewness
1	2013.09.01	0.29	0.07	-5	-0.5
2	2013.05.30	0.17	0.03	+40	2.0
3	2013.11.03	0.19	0.03	-28	-3.0
4	2013.06.05	0.30	0.06	+16	+2.2
5	2013.09.11	0.10	0.01	-60	-2.4
6	2013.07.23	0.10	0.02	+57	+2.7
7	2013.04.24	0.34	0.11	-26	-1.7
8	2013.02.27	0.29	0.05	-34	-3.2
9	2013.09.29	0.13	0.03	-46	-2.9
10	2014.01.01	0.41	0.04	+13	+1.1
11	2014.03.20	0.20	0.05	+20	+1.4
12	2014.02.05	0.31	0.07	-14	-0.9
13	2014.07.08	0.38	0.07	-9	+1.3
14	2014.01.09	0.19	0.03	-37	-2.0
15	2014.10.18	0.22	0.07	+31	+2.6
16	2014.07.24	0.36	0.06	-29	-3.4
17	2014.02.25	0.10	0.01	-61	-2.7
18	2014.09.24	0.10	0.01	+68	+2.7
19	2015.06.20	0.19	0.01	+39	+2.7
20	2015.08.20	0.21	0.01	+33	+2.3
21	2015.10.05	0.17	0.03	+37	+2.5
22	2015.12.08	0.15	0.02	+43	+3.1
23	2015.03.10	0.22	0.07	-35	-2.8
24	2015.02.11	0.17	0.02	-36	-2.7
25	2015.06.11	0.17	0.03	+28	+2.3
26	2015.08.13	0.14	0.02	+49	+4.9
27	2015.04.18	0.19	0.03	+32	+2.2
28	2015.03.31	0.10	0.02	+56	+2.8
29	2016.08.01	0.18	0.03	+36	+1.8
30	2016.06.02	0.23	0.02	-35	-1.9
31	2016.05.07	0.33	0.07	-13	-0.5
32	2016.11.10	0.27	0.07	-21	-2.1
33	2016.10.14	0.22	0.04	-21	-1.9
34	2016.12.20	0.30	0.10	+18	+1.8
35	2016.07.26	0.25	0.05	-22	-1.2
36	2016.10.26	0.53	0.09	+11	+1.5
37	2016.09.29	0.31	0.07	+17	+2.5
38	2017.01.03	0.28	0.03	-16	-0.4
39	2017.07.06	0.09	0.01	+54	+2.9
40	2017.01.17	0.29	0.06	+11	-0.3
41	2017.11.17	0.25	0.05	+27	+2.8
42	2017.03.20	0.40	0.06	+19	+2.7
43	2017.02.21	0.23	0.03	+30	+2.8
44	2017.04.22	0.26	0.07	-28	-2.3
45	2017.12.22	0.21	0.03	+26	+0.7
46	2017.09.25	0.26	0.06	+18	+1.3
47	2018.09.05	0.20	0.03	-28	-2.6
48	2018.10.05	0.27	0.04	+21	+2.7

**Table 1** (continued)

CH nr	Date (yyyy. mm.dd)	Cancellation expo- nent $k$	$\Delta$	Mean (G)	Skewness
49	2018.05.03	0.18	0.02	-30	-1.8
50	2018.11.08	0.25	0.06	-18	-1.2
51	2018.02.14	0.25	0.06	-25	-2.3
52	2018.04.17	0.29	0.05	-24	-2.3
53	2018.01.18	0.29	0.07	-23	-1.3
54	2018.03.13	0.19	0.05	-34	-2.1
55	2018.05.30	0.39	0.11	-19	-0.7
56	2019.07.02	0.23	0.03	-29	-3.0
57	2019.08.02	0.39	0.09	+22	+1.6
58	2019.01.21	0.41	0.10	+16	+1.7
59	2019.10.23	0.29	0.06	+11	-1.0
60	2019.09.25	0.25	0.07	+29	+3.3

does not affect significantly the results. This result has been verified reporting the scale of the first plateau point using two thresholds:  $10^{-4}$  and  $10^{-6}$ . We have also calculated the position at which the plateau is triggered averaging the first point of the plateau with the previous one.

For the CH case we find (for both the used thresholds) that the 83% of the CHs have a plateau that starts at  $36 \pm 12$  Mm. In the case of the NCHs only the 13% of the selected regions present this plateau (using the first threshold; with the second threshold the value is 10%).

From the distributions analysis we also confirm that CH photospheric magnetic fields are imbalanced: in Fig. 4 we report the distribution of the means of the photospheric magnetic fields of the CHs (upper panel) and of the NCHs (lower panel) regions. From the comparison of the two distributions we can deduce that higher values of the means in the case of CHs are more probable.

In Fig. 5 we report the distribution of the skewness of the photospheric magnetic fields of the CHs (upper panel) and of the NCHs (lower panel) regions. As seen for the average, higher values of the skewness are more common for regions associated to the CHs, finally indicating that radial magnetic fields are imbalanced in the polarity.

## 4 Conclusion

The classical definition of coronal holes is that they appear as dark regions in the solar corona in extreme ultraviolet and soft x-ray solar disk images. Moreover, they are generally associated with open magnetic fields and this topology is due to the imbalance of the magnetic flux density in their photospheric counterpart. Carefully defining the scale at which this imbalance originates is of high interest

**Table 2** Analyzed non coronal hole regions

CH nr	Date (yyyy. mm.dd)	Cancellation exponent $k$	$\Delta$	Mean ( $G$ )	Skewness
1	2019.10.01	0.37	0.06	-4	-1.9
2	2020.05.02	0.29	0.07	-5	-0.7
3	2019.05.03	0.22	0.04	-26	-2.7
4	2020.02.04	0.28	0.08	+2	+0.5
5	2020.03.04	0.47	0.07	+11	+3.3
6	2020.04.04	0.53	0.07	-9	-0.4
7	2019.10.04	0.31	0.05	-4	-0.8
8	2019.12.06	0.26	0.05	-2	-0.7
9	2019.01.07	0.19	0.02	-25	-0.9
10	2020.05.07	0.26	0.03	-7	-1.2
11	2020.01.08	0.30	0.07	+8	+1.1
12	2019.04.08	0.42	0.07	-5	+0.8
13	2020.10.08	0.51	0.15	-12	-1.5
14	2019.11.09	0.28	0.06	+6	-0.2
15	2019.12.09	0.44	0.10	-20	-2.6
16	2020.02.10	0.40	0.06	-15	-1.5
17	2020.04.10	0.37	0.09	+3	+2.5
18	2019.10.10	0.76	0.23	-1	-0.7
19	2020.03.13	0.31	0.06	-5	-0.1
20	2019.06.13	0.33	0.09	-6	-0.3
21	2019.02.14	0.42	0.09	+2	-0.5
22	2019.10.14	0.46	0.09	-3	-0.1
23	2020.08.15	0.43	0.06	-2	-1.1
24	2019.09.15	0.38	0.06	-7	-0.7
25	2020.12.15	0.27	0.06	+11	+1.4
26	2019.01.16	0.48	0.08	-1	+0.2
27	2020.01.16	0.21	0.05	+4	-0.5
28	2020.02.16	0.24	0.05	-5	+0.5
29	2019.07.16	0.26	0.07	+6	+0.5
30	2020.03.17	0.46	0.10	0	-1.2
31	2019.05.17	0.26	0.04	-15	-2.5
32	2020.05.18	0.34	0.06	+1	-0.1
33	2019.09.18	0.22	0.05	+5	+2.9
34	2019.11.18	0.78	0.18	+1	-0.7
35	2020.01.20	0.48	0.12	-13	-1.2
36	2020.02.20	0.30	0.07	0	+0.4
37	2019.06.20	0.64	0.17	-4	-0.4
38	2020.06.20	0.25	0.06	-11	-2.5
39	2019.07.20	0.34	0.04	-3	0.0
40	2020.03.21	0.50	0.13	+3	+0.8
41	2019.04.22	0.29	0.07	-4	+1.1
42	2020.05.22	0.35	0.09	+22	+1.3
43	2020.08.22	0.64	0.16	-4	+0.5
44	2019.05.23	0.30	0.06	-7	+0.1
45	2020.01.25	0.51	0.11	+3	-0.1
46	2020.02.25	0.32	0.10	5	0.0
47	2020.03.25	0.33	0.06	-8	-0.6
48	2019.04.25	0.33	0.11	+2	+1.0

**Table 2** (continued)

CH nr	Date (yyyy. mm.dd)	Cancellation exponent $k$	$\Delta$	Mean ( $G$ )	Skewness
49	2019.06.26	0.53	0.19	-9	-0.1
50	2019.11.27	0.31	0.06	-2	-0.8
51	2019.09.28	0.49	0.09	-5	-0.3
52	2019.05.29	0.36	0.03	-16	-2.8
53	2020.02.29	0.50	0.07	+6	+0.2
54	2019.06.29	0.45	0.11	+7	+1.5
55	2019.03.30	0.43	0.12	+3	0.0
56	2020.03.30	0.66	0.20	+10	+1.3
57	2020.05.30	0.49	0.10	-6	-0.6
58	2019.10.30	0.44	0.06	0	0.0
59	2019.11.30	0.50	0.09	+2	+0.4
60	2019.12.30	0.28	0.11	+3	+0.3

to understand the origin of CHs and the physical processes connected to the acceleration of the high speed solar wind whose effects on space weather are relevant in the circum-terrestrial environment.

Comparing the properties of the photospheric magnetic fields associated to CH and NCH regions we have confirmed that CHs magnetic fields are imbalanced in the sign.

Moreover, from the cancellation analysis we have estimated the cancellation index for the two classes of regions, i.e. CHs and NCHs, obtaining smaller values for CH fields. This result tells us that photospheric magnetic fields in Coronal Holes are smoother in the sign, i.e. oscillate less with respect to NCH regions.

However, the most important result of this work, which derives from the sign singularity analysis applied to the magnetograms associated with CHs, consists in having quantitatively measured the scale at which the imbalance in the sign of the magnetogram emerges. In the CHs this imbalance emerges mainly from the supergranular scale (about 30 Mm) (e.g. Berrilli et al. 2004; Giannattasio et al. 2018). This result strongly supports the hypothesis that the origin of the CHs is the organization of the magnetic field of defined polarity along the edges of the supergranular structures.

Our findings supports the idea, reported in literature, e.g.: Hofmeister et al. (2017), that the largest part of CHs magnetic flux imbalance emerges from small areas and that this imbalance is caused mainly by long lived magnetic patches (that could be reasonably associated to the supergranular network) Hofmeister et al. (2019).

Finally, we must underline that our results are compatible with the hypothesis that the footpoints of the open coronal magnetic fields (the funnels) from which the fast solar wind originates (Tu et al. 2005) are rooted in the supergranular network.

**Acknowledgements** This paper is partially based on Master's thesis research "Cancellation properties in quiet-Sun photosphere hosting Coronal Holes and ephemeral regions" conducted by M.C. under the supervision of Prof. F. Berrilli. M.C. was supported by the Joint Research PhD Program in Astronomy, Astrophysics and Space Science between the universities of Roma Tor Vergata, Roma Sapienza, and INAF. The authors are sincerely indebted to Professor V. Carbone and Dr. G. Consolini for their suggestions in the use of signed measure analysis. Data are courtesy of NASA/SDO and the AIA and HMI science teams.

**Funding** Open access funding provided by Università degli Studi di Roma Tor Vergata within the CRUI-CARE Agreement.

**Open Access** This article is licensed under a Creative Commons Attribution 4.0 International License, which permits use, sharing, adaptation, distribution and reproduction in any medium or format, as long as you give appropriate credit to the original author(s) and the source, provide a link to the Creative Commons licence, and indicate if changes were made. The images or other third party material in this article are included in the article's Creative Commons licence, unless indicated otherwise in a credit line to the material. If material is not included in the article's Creative Commons licence and your intended use is not permitted by statutory regulation or exceeds the permitted use, you will need to obtain permission directly from the copyright holder. To view a copy of this licence, visit <http://creativecommons.org/licenses/by/4.0/>.

## References

- Abramenko VI, Fisk LA, Yurchyshyn VB (2006) The rate of emergence of magnetic dipoles in coronal holes and adjacent quiet-sun regions. *Astrophys J* 641(1):65–68. <https://doi.org/10.1086/503870>
- Berrilli F, Del Moro D, Consolini G, Pietropaolo E, Duvall JTL, Kosovichev AG (2004) Structure properties of supergranulation and granulation. *Solar Phys* 221(1):33–45. <https://doi.org/10.1023/B:SOLA.0000033368.00217.de>
- Berrilli F, Scardigli S, Giordano S (2013) Multiscale magnetic underdense regions on the solar surface: granular and mesogranular scales. *Solar Phys* 282(2):379–387. <https://doi.org/10.1007/s11207-012-0179-2>. arXiv:1208.2669 [astro-ph.SR]
- Berrilli F, Scardigli S, Del Moro D (2014) Magnetic pattern at supergranulation scale: the void size distribution. *Astron Astrophys* 568:102. <https://doi.org/10.1051/0004-6361/201424026>. arXiv:1406.5871 [astro-ph.SR]
- Cadavid A, Lawrence J, Ruzmaikin A, Kayleng-Knight A (1994) Multifractal models of small-scale solar magnetic fields. *Astrophys J* 429:391–399
- Carbone V, Bruno R (1997) Sign singularity of the magnetic helicity from in situ solar wind observations. *Astrophys J* 488(1):482. <https://doi.org/10.1086/304670>
- Cicogna D, Berrilli F, Calchetti D, Del Moro D, Giovannelli L, Benvenuto F, Campi C, Guastavino S, Piana M (2021) Flare-forecasting algorithms based on high-gradient polarity inversion lines in active regions. *Astrophys J* 915(1):38. <https://doi.org/10.3847/1538-4357/abfab>. arXiv:2105.00897 [astro-ph.SR]
- Consolini G, Lui ATY (1999) Sign-singularity analysis of current disruption. *Geophys Res Lett* 26(12):1673–1676. <https://doi.org/10.1029/1999GL900355>
- Consolini G, De Michelis P, Coco I, Alberti T, Marcucci MF, Giannattasio F, Tozzi R (2021) Sign-singularity analysis of field-aligned currents in the ionosphere. *Atmosphere*. <https://doi.org/10.3390/atmos12060708>
- Couvidat S, Schou J, Hoeksema JT, Bogart RS, Bush RI, Duvall TL, Liu Y, Norton AA, Scherrer PH (2016) Observables processing for the helioseismic and magnetic imager instrument on the solar dynamics observatory. *Solar Phys* 291(7):1887–1938. <https://doi.org/10.1007/s11207-016-0957-3>. arXiv:1606.02368 [astro-ph.SR]
- Cranmer SR (2009) Coronal holes. *Liv Rev Solar Phys* 6(1):3. <https://doi.org/10.12942/lrsp-2009-3>. arXiv:0909.2847 [astro-ph.SR]
- Fisk LA (2005) The open magnetic flux of the sun. I. Transport by reconnections with coronal loops. *Astrophys J* 626(1):563–573. <https://doi.org/10.1086/429957>
- Giannattasio F, Berrilli F, Consolini G, Del Moro D, Gošić M, Bellot Rubio L (2018) Occurrence and persistence of magnetic elements in the quiet sun. *Astron Astrophys* 611:56. <https://doi.org/10.1051/0004-6361/201730583>. arXiv:1801.03871 [astro-ph.SR]
- Hagenaar HJ, DeRosa ML, Schrijver CJ (2006) The dependence of ephemeral region emergence on local flux imbalance. *Astrophys J* 678(1):541–548. <https://doi.org/10.1086/533497>
- Heinemann SG, Temmer M, Hofmeister SJ, Veronig AM, Vennerstrøm S (2018a) Three-phase evolution of a coronal hole. I. 360° Remote sensing and in situ observations. *Astrophys J* 861(2):151. <https://doi.org/10.3847/1538-4357/aac897>. arXiv:1806.09495 [astro-ph.SR]
- Heinemann SG, Hofmeister SJ, Veronig AM, Temmer M (2018b) Three-phase evolution of a coronal hole. II. The magnetic field. *Astrophys J* 863(1):29. <https://doi.org/10.3847/1538-4357/aad095>. arXiv:1806.10052 [astro-ph.SR]
- Heinemann SG, Jerčić V, Temmer M, Hofmeister SJ, Dumbović M, Vennerstrom S, Verbanac G, Veronig AM (2020) A statistical study of the long-term evolution of coronal hole properties as observed by SDO. *Astron Astrophys* 638:68. <https://doi.org/10.1051/0004-6361/202037613>. arXiv:1907.02795 [astro-ph.SR]
- Hofmeister SJ, Veronig A, Reiss MA, Temmer M, Vennerstrom S, Vršnak B, Heber B (2017) Characteristics of low-latitude coronal holes near the maximum of solar cycle 24. *Astrophys J* 835(2):268. <https://doi.org/10.3847/1538-4357/835/2/268>. arXiv:1702.02050 [astro-ph.SR]
- Hofmeister SJ, Utz D, Heinemann SG, Veronig A, Temmer M (2019) Photospheric magnetic structure of coronal holes. *Astron Astrophys* 629:22. <https://doi.org/10.1051/0004-6361/201935918>. arXiv:1909.03806 [astro-ph.SR]
- Karachik N, Pevtsov A, Abramenko V (2010) Formation of coronal holes on the ashes of active regions. In: American Astronomical Society Meeting Abstracts, vol. 216, pp 401–404
- Lawrence JK, Ruzmaikin AA, Cadavid AC (1993) Multifractal measure of the solar magnetic field. *Astrophys J* 417:805. <https://doi.org/10.1086/173360>
- Mackay DH, Yeates AR (2012) The sun's global photospheric and coronal magnetic fields: observations and models. *Liv Rev Solar Phys* 9(1):6. <https://doi.org/10.12942/lrsp-2012-6>. arXiv:1211.6545 [astro-ph.SR]
- Napoletano G, Foldes R, Camporeale E, de Gasperis G, Giovannelli L, Paouris E, Pietropaolo E, Teunissen J, Tiwari AK, Del Moro D (2022) Parameter distributions for the drag-based modeling of CME propagation. *Sp Weather* 20(9):2021–002925. <https://doi.org/10.1029/2021SW002925>. arXiv:2201.12049 [physics.space-ph]
- Ott E, Du Y, Sreenivasan KR, Juneja A, Suri AK (1992) Sign-singular measures: Fast magnetic dynamos, and high-Reynolds-number fluid turbulence. *Phys Rev Lett* 69(18):2654–2657. <https://doi.org/10.1103/PhysRevLett.69.2654>
- Pesnell WD, Thompson BJ, Chamberlin PC (2012) The solar dynamics observatory (SDO). *Astrophys J* 775(1–2):3–15. <https://doi.org/10.1007/s11207-011-9841-3>
- Plainaki C, Antonucci M, Bemporad A, Berrilli F, Bertucci B, Castro-nuovo M, De Michelis P, Giardino M, Iuppa R, Laurenza M,

- Marcucci F, Messerotti M, Narici L, Negri B, Nozzoli F, Orsini S, Romano V, Cavallini E, Polenta G, Ippolito A (2020) Current state and perspectives of Space Weather science in Italy. *J Sp Weather Sp Clim* 10:6. <https://doi.org/10.1051/swsc/2020003>
- Plutino N, Berrilli F, Del Moro D, Giovannelli L (2023) A new catalogue of solar flare events from soft X-ray GOES signal in the period 1986–2020. *Adv Sp Res* 71(4):2048–2058. <https://doi.org/10.1016/j.asr.2022.11.020>. arXiv:2211.10189 [astro-ph.SR]
- Ruzmaikin AA, Lawrence JK, Cadavid AC (1993) Multiscale measure of the solar magnetic field. In: *Bulletin of the American Astronomical Society*, vol. 25, p 1219
- Scardigli S, Berrilli F, Del Moro D, Giovannelli L (2021) Stellar turbulent convection: the multiscale nature of the solar magnetic signature. *Atmosphere* 12(8):938. <https://doi.org/10.3390/atmos12080938>
- Sorriso-Valvo L, Abramenko V, Carbone V, Noullez A, Politano H, Pouquet A, Veltri P, Yurchyshyn V (2003) Cancellations analysis of photospheric magnetic structures and flares. 74:631
- Sorriso-Valvo L, De Vita G, Kazachenko MD, Krucker S, Primavera L, Servidio S, Vecchio A, Welsch BT, Fisher GH, Lepreti F, Carbone V (2015) Sign singularity and flares in solar active region NOAA 11158. *Astrophys J* 801(1):36. <https://doi.org/10.1088/0004-637X/801/1/36>. arXiv:1501.04279 [astro-ph.SR]
- Tu C-Y, Zhou C, Marsch E, Xia L-D, Zhao L, Wang J-X, Wilhelm K (2005) Solar wind origin in coronal funnels. *Science* 308(5721):519–523. <https://doi.org/10.1126/science.1109447>
- Verbeeck C, Delouille V, Mampaey B, De Visscher R (2014) The SPoCA-suite: Software for extraction, characterization, and tracking of active regions and coronal holes on EUV images. *Astron Astrophys* 561:29. <https://doi.org/10.1051/0004-6361/201321243>
- Wang Y-M (2009) Coronal holes and open magnetic. *Flux* 144(1–4):383–399. <https://doi.org/10.1007/s11214-008-9434-0>
- Wang Y-M (2020) Small-scale flux emergence, coronal hole heating, and flux-tube expansion: a hybrid solar wind model. *Astrophys J* 904(2):199. <https://doi.org/10.3847/1538-4357/abbda6>. arXiv:2104.04016 [astro-ph.SR]
- Wiegelmann T, Thalmann JK, Solanki SK (2014) The magnetic field in the solar atmosphere. *Astron Astrophys Rev* 22:78. <https://doi.org/10.1007/s00159-014-0078-7>. arXiv:1410.4214 [astro-ph.SR]
- Zhai XM, Sreenivasan KR, Yeung PK (2019) Cancellation exponents in isotropic turbulence and magnetohydrodynamic turbulence. *Phys Rev E* 99:023102. <https://doi.org/10.1103/PhysRevE.99.023102>

**Publisher's Note** Springer Nature remains neutral with regard to jurisdictional claims in published maps and institutional affiliations.